PHYSICAL REVIEW B 80, 045207 (2009)

Observation of precursor pair formation of recombining charge carriers

Jan Behrends* and Klaus Lips
Institut für Silizium-Photovoltaik, Helmholtz-Zentrum Berlin für Materialien und Energie (formerly Hahn-Meitner-Institut), Kekuléstr 5, D-12489 Berlin, Germany

Christoph Boehme
Department of Physics, University of Utah, 115S 1400E, Salt Lake City, Utah 84112, USA
(Received 20 December 2008; revised manuscript received 18 May 2009; published 15 July 2009)

An experiment is presented which allows the observation of charge-carrier pair formation that precedes electronic transitions such as spin-dependent recombination or spin-dependent transport. It is based on an electrically detected magnetic-resonance-induced rotary echo sequence. The experimental demonstration is performed on precursor (spin) pairs of electrons in the emitter layer of crystalline silicon/amorphous silicon heterostructures. Precursor pair-generation-rate coefficients extracted from these measurements are studied as a function of light intensity and are found to show only a minor dependence on the illumination level indicating that the pair generation is not determined by charge-carrier densities.

DOI: 10.1103/PhysRevB.80.045207 PACS number(s): 72.20.Jv, 72.20.Ee, 73.50.Gr, 76.60.Lz

I. INTRODUCTION

Transitions of charge carriers through localized electronic states occur in various qualitatively and quantitatively different forms such as defect or excitonic recombination processes or hopping transport in disordered materials. Common to all these processes is that they take place through multiple electronic transitions which involve the formation of intermediate pairs in one or several localization steps before the final recombination or transport transitions occur. Examples for such processes are defect recombination described by Shockley and Read[1] for which intermediate pairs are crucial to exist even though they can often be neglected for the statistical Shockley-Read-Hall description of recombination. Other examples include excitonic recombination for which the excitonic states represent intermediate pairs,[2] excitonic recombination through additional precursor states as observed in many organic semiconductor systems[3] or hopping transport in the low-temperature regime of disordered semiconductors[4] where precursor pairs are constituted by nearest-neighbor arrangements. The influence of the precursor states for macroscopic electrical or optical properties is oftentimes negligible, yet there are some exceptions where the nature of the precursor pairs and their formation profoundly affect transport or recombination. For these systems, the ability to experimentally access precursor pair-generation rates becomes crucial for the understanding of their microscopic nature. Examples for this often involve spin-dependent transitions that can be found in weakly spin-orbital-coupled materials (e.g., in any known silicon morphology[4] or organic semiconductors[3,5]) since the precursor pair formation determines, for these cases, macroscopic material and device properties such as magnetoresistance[6] or device efficiency.[7]

In the following, we present an experiment which allows the observation of the precursor pair formation for spin-dependent transport and recombination processes. This experiment is based on the observation of coherent spin motion of precursor pairs using a pulsed electrically detected magnetic-resonance (pEDMR) induced rotary echo pulse sequence. EDMR measures changes in the (photo) conductivity of a semiconductor material resulting from magnetic-resonant alteration of transition rates of spin pairs. Independent of the specific type of microscopic transition process—either spin-dependent hopping, trapping, or recombination—intermediate spin pairs[8–10] (precursor pairs) consisting of two charge carriers with spin $S=1/2$ determine the observed signals. EDMR-detected rotary echoes are produced by spin ensembles which are dephased from an initial eigenstate due to a resonantly induced inhomogeneous spin nutation (a so-called pulse-induced Rabi nutation) before they are rephased due to a second pulse with opposite phase.[11]

Rotary echoes have been used in the past for the measurement of precursor pair coherence times as the decay of a rotary echo train poses a limit on the net decay rate caused by precursor pair recombination or dissociation.[12] However, it is difficult to distinguish experimentally between different possible influences that can affect the echo decay, among them (a) transitions that destroy spin-pair coherence (either hopping, recombination, or trapping), (b) spin relaxation, (c) dissociation, and (d) precursor pair generation during the experiment. While the theoretical models describing pEDMR have been tested experimentally with regard to dissociation, hopping, and recombination dynamics,[4,10,13] the process of precursor pair generation is complicated to access experimentally. Usually, spin-pair generation is assumed to be negligible during the microwave (mw) excitation in a pEDMR experiment. This is certainly justified for the typical current relaxation and transient nutation experiments where only one short microwave pulse with a length of a few 100 ns is used. In contrast to that, spin-pair generation can become important for more advanced (and much longer) pulse sequences. Furthermore, spin-pair generation influences pEDMR signals on the time scale where current relaxation transients (the basis of all pEDMR experiments) are recorded.[10] Note that, however, neither the decay of the rotary echo nor the transient behavior of the observed EDMR signals reveals infor-

mation about the pair-generation rate as precursor pair-generation rates are only weakly dependent on the rate changes induced by magnetic resonance (see arguments made in Refs. 10, 14, and 15). Therefore, measuring the dynamics of precursor pair generation has remained elusive so far.

For the experiment presented, the problem is solved by measuring the Rabi nutation around a rotary echo signal as a function of a separation time between dephasing and rephasing of the spin ensemble. It is shown that one can distinguish the pEDMR signals from precursor pairs which existed before the dephasing pulse from those generated after the pulse due to a 180° phase difference of the Rabi nutation signals which originate from the two ensembles. Thus, a disentanglement of true loss of coherence [effects (a)–(c) as mentioned before] and spin-pair generation (d) can be achieved.

The demonstration of this experiment was conducted on a heterostructure solar cell consisting of a highly phosphorus-doped hydrogenated amorphous silicon (a-Si:H) emitter layer and a crystalline silicon (c-Si) absorber. These heterostructures are known to exhibit a strong pEDMR signal resulting from hopping of electrons via localized conduction-band tail and phosphorus states in the a-Si:H layer.[4,16] Changes in the precursor pair-generation rate caused by a light-flux-controlled change in the charge-carrier generation rate are investigated. While pEDMR was used for the experiments presented here, it shall be stressed that this experiment could conceivably be carried out in an equal way (using the same magnetic-resonance pulse sequence) for the investigation of optically detected spin-dependent transitions using photoluminescent or electroluminescent processes.[17,18]

II. ELECTRICALLY DETECTED ROTARY ECHO

The experiment is started from the steady state where all electronic transition rates are constant. Therefore, precursor pairs are constantly generated and their influence on an observed rate (referred to as I_{ph} since we use a photocurrent for the experiments presented) is balanced by the annihilation of spin pairs through processes such as dissociation, hopping, or recombination. In the steady state, the number of pairs, and therefore I_{ph}, are constant in time. When applying a resonant mw pulse, the spin pairs will begin a coherent nutation (a Rabi oscillation) and their phase coherence will be lost gradually due to spin relaxation, spin-dependent electronic pair decay, and inhomogeneous magnetic fields. When further spin pairs are formed during the application of this pulse, these spin pairs will be generated in eigenstates and thus, due to their random time of generation, they will be at random phase to the already existing spin-pair ensemble. Thus, spin-pair generation will influence the signal in a similar way like any other source of decoherence. This can be studied by utilizing the pulse sequence illustrated in Fig. 1 which consists of two subsequent pulses with opposite (180°) phase relation.

During the first pulse, the spin ensemble carries out a gradually dephasing Rabi nutation which can be observed with pEDMR by measurement of the integrated charge $Q(\tau)$ after the pulse as a function of the applied pulse length τ

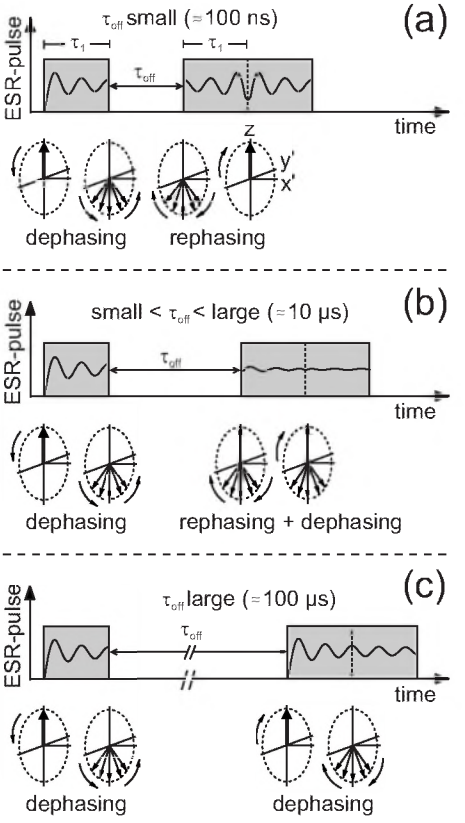

FIG. 1. Sketch of the rotary echo experiment that can be used to study precursor pair generation. The pulse sequence consists of two microwave pulses with opposite phase and an interpulse waiting time, τ_{off}. The sketch illustrates three cases: (a) for τ_{off} much shorter than the pair-generation time, (b) for τ_{off} of the order of the generation time and (c) for τ_{off} much longer than the pair-generation time. The time traces are drawn along with the dephasing states of the spin ensemble at the beginning and the end of each pulse. The Rabi oscillation of the spins reflected by the pEDMR signal $Q(\tau_{1,2})$, as plotted for the gray shaded time interval during the pulses, is phase inverted for pairs generated during the interpulse time in comparison to pairs generated before the pulse sequence begins. Hence, the deconvolution of the Rabi oscillation into phase inverted and non-phase inverted oscillation components allows a relative quantification of newly generated pairs and pre-existent pairs. For details see text.

(Ref. 4). $Q(\tau)$, which is obtained by integrating the current transient after the mw excitation, represents a projection of the spin state of the precursor pair at the end of the pulse. For the pulse sequence in Fig. 1, the length of the first pulse is kept at constant length τ_1 and $Q(\tau_2)$ is measured as a function of the length τ_2 of the second pulse which now represents initially (for $\tau_2 < \tau_1$) a dephased Rabi oscillation that gradually recovers to the rotary echo at $\tau_2 = \tau_1$ before it dephases again at $\tau_2 > \tau_1$. Note that this detection scheme for rotary echoes was used for the first electrical detection of spin coherence[12] and has since then been applied to various studies on decay processes of precursor pairs.[17,19,20] It shall be noted that rotary echoes are always observed at a time $\tau_2 = \tau_1$, independently of the length τ_1 of the initial dephasing pulse.

For the observation of the generation of precursor pairs we now set the length τ_1 to a value so that the corresponding flip angle of the spin ensemble is $(2n+1)\pi$ with n being an integer number (the flip angle is 5π in the sketched experiment) and we also introduce an interpulse waiting time, τ_{off}, between the two pulses during which the dephased spin ensemble remains completely unchanged in a rotating Bloch sphere representation, as long as no pairs decay and no new pairs are generated. The length τ_2 of the second pulse is again incremented gradually so that the integrated sample current $Q(\tau_2)$ measured after the two pulses as a function of τ_2 reflects the rephasing Rabi oscillation due to the rotary echo.

The expected pEDMR signal $Q(\tau_2)$ is depicted inside the gray shaded pulse intervals in Fig. 1 for three different interpulse waiting times: (a) for a short τ_{off}, almost all spins that have dephased during pulse 1 can be refocused during the second pulse. The echo signal corresponds to a (local) minimum of $Q(\tau_2)$ for $\tau_2=\tau_1$. (b) For larger values of τ_{off} the spin pairs that are generated between the two mw pulses significantly influence $Q(\tau_2)$ in addition to spin pairs that are lost during τ_{off} due to annihilation (dissociation or recombination). While the surviving spin pairs that are refocused during pulse 2 again result in a minimum signal, the newly generated spin pairs give rise to a maximum at $\tau_2=\tau_1$ as the flip angle of the newly generated spins is $(2n+1)\pi$. Thus, the measured signal is a combination of two 180° phase-shifted oscillations. When the ensemble of newly generated pairs equals the ensemble of previously generated pairs, the two signals compensate each other at the time of the echo. (c) When τ_{off} is sufficiently long so that the coherent information generated during the first pulse is lost due to spin-pair annihilation, the signal measured is completely determined by spin pairs that have been generated during τ_{off}. Hence, the signal is the same like the signal obtained in a Rabi oscillation measurement without the first pulse and, therefore, it exhibits a clear maximum at $\tau_2=\tau_1$.

By fitting model functions to the experimental results of $Q(\tau_2)$ for various τ_{off}, the relative magnitudes of the ensemble sizes of the newly and previously generated precursor pairs can be obtained as a function of τ_{off}, and these dependencies represent both the generation and decay dynamics of the precursor pairs, respectively. This procedure is demonstrated in Sec. V using experimentally obtained pEDMR rotary echo signals.

It shall be mentioned that the magnitude of the rotary echo is always affected by the distribution of Larmor frequencies which will result in a dephasing contribution that cannot be rephased with the method presented here. This "lost" part of the spin-pair ensemble is always equal for a given experiment and it will therefore always superimpose the $Q(\tau_2)$. It is therefore not relevant for the evaluation of decay times from the observed echo amplitude dependence of τ_{off}. It shall be noted though that Larmor rephasing is possible by means of a pEDMR Hahn echo experiment.[21]

III. EXPERIMENTAL DETAILS

Figure 2 shows sketches of the a-Si:H/c-Si heterostructure

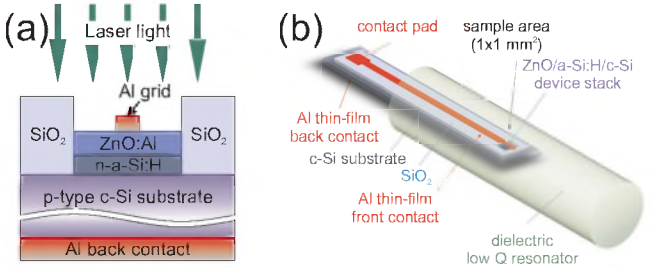

FIG. 2. (Color online) (a) Cross-section of the heterostructure solar cell and (b) geometrical sketch of the entire pEDMR sample. The sample consists of 2×50 mm^2 of a boron doped crystalline silicon wafer which provides the absorber of the cell. The phosphorus doped amorphous silicon (emitter layer) and the ZnO (transparent conducting oxide) cover only a square of 1×1 mm^2. A window of the same size was etched out of the SiO_2 before the deposition. The front contact (Al grid finger) is connected to a thin-film strip line that extends to the opposite side of the substrate. Electrical isolation from the crystalline silicon is accomplished by the SiO_2. Structuring of the sample was done using standard optical lithography. For the pEDMR experiments the sample is illuminated through the a-Si:H side.

used for the experiments in this study. Technologically, this device represents a solar cell. A 220-μm-thick boron-doped c-Si substrate with (100) surface orientation was used as absorber. The emitter layer, consisting of 20 nm phosphorous-doped a-Si:H, was deposited on top of the c-Si substrate using plasma-enhanced chemical vapor deposition. 80 nm of highly Al-doped ZnO serves as transparent conducting oxide and is connected to a 100-μm-wide and 200-nm-thick Al front contact finger. A 200-nm-thick Al back contact layer was deposited on the opposite side of the c-Si substrate. The active area of the solar cell was confined to 1 mm^2 resulting from the size of a window that was etched out of approximately 500 nm thermally grown SiO_2 covering the c-Si. The Al back contact as well as the Al front contact finger, which is electrically isolated from the c-Si by SiO_2, extend to the end of the substrate (size 50×2 mm^2). This thin-film wiring is indispensable in order to minimize artifacts induced by strong mw bursts used in the experiment and in order to not perturb the eigenmodes of the dielectric microwave resonator by the electrical circuitry. Several sample structures were processed on one wafer in parallel. They were cut into the appropriate size after the last processing step. Solar cells deposited in a similar manner were shown to reach efficiencies above 17% (cf. Ref. 22) for a solar cell area of 1 cm^2.

All measurements were carried out in a Bruker E580 X-band electron spin resonance (ESR) spectrometer. The sample was held at $T=10$ K using a continuous flow helium cryostat. In order to facilitate a current which is sufficiently high for a pEDMR experiment, excess charge carriers were created optically by monochromatic light ($\lambda=514$ nm) from an Argon-ion laser. The generation rate of free charge carriers in the sample could be changed by adjusting the optical output power of the laser. The light was fed through an optical fiber ending above the active sample area. A constant current source (Keithley 220PCS) was used to establish a constant photocurrent, $I_{\text{ph}}=-1$ μA, corresponding to a current density of -0.1 mA cm^{-2} (reverse bias regime of the

solar cell). Hence, optically generated electrons and holes in both the a-Si:H layer and the c-Si wafer are extracted through the Al contacts. The applied voltage which is required for $I_{ph}=-1$ μA depends on the photon flux and amounts to values between 0.04 and 0.27 V for the conditions used in the experiments. The response of the current source was slow compared to the time scale on which the pEDMR experiments were carried out, so that the ESR-induced current change, ΔI_{ph}, was not compensated.

In a pEDMR experiment the current transients after a mw excitation are recorded for several hundred microseconds for different values of the static magnetic field, B_0. Therefore, by analyzing ΔI_{ph} as function of time, t, after a mw pulse at fixed B_0 (in the following referred to as pEDMR transients), one can gain insight into the dynamics of spin-dependent processes, whereas ΔI_{ph} at fixed t (pEDMR spectrum) contains the spectral information which is also accessible by the well-established continuous-wave (cw) EDMR technique.[23,24]

IV. pEDMR ON a-Si:H/c-Si SOLAR CELLS

Figure 3(a) shows the pEDMR spectrum measured $t=10$ μs after excitation with a 320-ns-long mw pulse.

The relaxation of the photocurrent was recorded for 200 μs with a temporal resolution of 0.2 μs and averaging 5×10^4 transients for each value of B_0. The best fit to the pEDMR spectrum could be obtained by assuming a single Lorentzian line at $g=2.0048(5)$. This is in accordance with earlier measurements on the same type of samples.[16] The underlying process is associated with electron hopping via conduction-band tail states in a-Si:H (Refs. 9, 25, and 26), which also explains that directly after the mw pulse a positive change ΔI_{ph} is observed [see Fig. 3(b)]. The pEDMR spectrum is superimposed by two 25 mT split satellites that result from neutral phosphorus donor states, which lie in the same energy range as the conduction-band tail states. The phosphorus hyperfine splitting of 25 mT in amorphous silicon, which significantly differs from the 4.2 mT splitting known from crystalline silicon,[27] was originally determined by ESR (Ref. 28) and later also observed in EDMR.[16,29] The satellites cannot be observed in Fig. 3(a) because of the limited magnetic field range used in the experiment.

Besides the spectral information which alternatively could have been extracted from a cwEDMR experiment,[30] pEDMR allows to study the time dependence of the resonance signal. The dynamics of pEDMR transients, i.e., the relaxation of I_{ph} back into the steady state after a resonant mw pulse excitation, is influenced by the spin-pair recombination or hopping rates as well as precursor pair generation.[4] Figure 3(b) shows two pEDMR transients measured under different illumination conditions using a photon flux of $\phi_0=1\times10^{17}$ cm^{-2} s^{-1} and $\phi=8\times10^{17}$ cm^{-2} s^{-1}. The applied voltage was adjusted to yield $I_{ph}=-1$ μA in both cases (corresponding to 0.21 and 0.27 V, respectively). It should be noted that the small adjustment of the bias voltage did not change the charge-carrier extraction mechanism. The shape of the transients can be fitted when assuming a combination of two single exponential functions (one with positive and

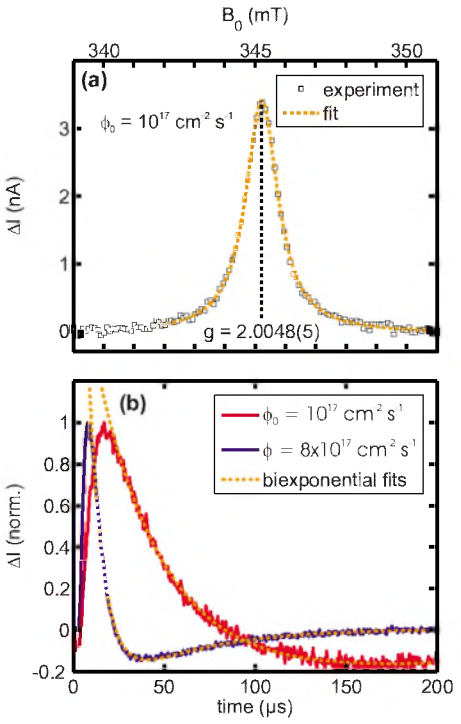

FIG. 3. (Color online) Results of a pEDMR experiment carried out at $T=10$ K using a photocurrent of $I_{ph}=-1$ μA. (a) Current change at $t=10$ μs after a 320-ns-long mw pulse (pEDMR spectrum). The spectrum reveals a single Lorentzian line at $g=2.0048(5)$ (dashed line) which in accordance with the g value of conduction-band tail states in amorphous silicon. The linewidth is dominated by power broadening resulting from the high mw power ($B_1\approx70$ μT) used in the experiment. (b) Current relaxation as a function of time after the mw excitation (pEDMR transient) on the resonance position at $g=2.0048(5)$ measured at two different light intensity levels as indicated in the legend. The dashed lines represent fits to the experimental data assuming a combination of two exponential functions for each transient. The respective time constants are given in the text.

one with negative amplitude) for each transient as inferred from theory [see dashed line in Fig. 3(b)].[10] The fits yield the time constants $\tau_a\approx40$ μs, $\tau_b\approx300$ μs and $\tau_a^*\approx8$ μs, $\tau_b^*\approx50$ μs for ϕ_0 and $8\times\phi_0$, respectively. It is tempting to associate the change in the two time constants upon increasing the photon flux with a rate change in the underlying microscopic mechanisms. However, although it is apparent that the photon flux certainly has a dramatic impact on the time constants, its interpretation with regard to spin-dependent transitions or precursor pair-generation-rate coefficients is not straightforward as the shape of pEDMR transients can also be affected by RC time constants of the detection electronics or the dielectric relaxation times of sample (for a more detailed analysis see Ref. 31).

An elegant way to study microscopic processes in pEDMR without any influence of RC time constants or other artifacts is to investigate the coherent spin motion during the mw excitation using a pulse-length-dependent measurement.[10] Figure 4(a) shows the charge response $Q(\tau)=\int_{3\ \mu s}^{19\ \mu s}\Delta I_{ph}dt$ determined at $g=2.0048$, i.e., at the maximum position of the resonance line shown in Fig. 3(a). These

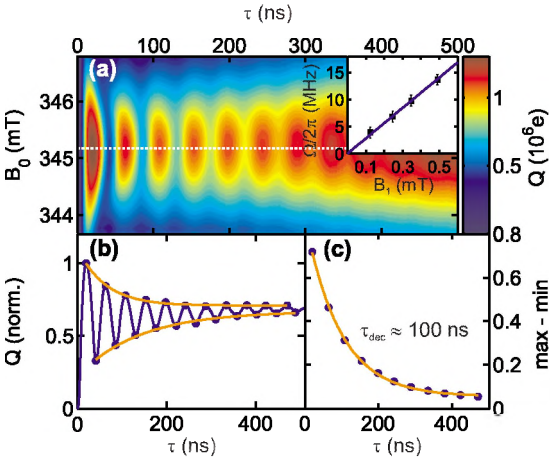

FIG. 4. (Color online) Observation of spin Rabi nutation performed at a steady-state photocurrent of $I_{ph}=-1$ μA at $T=10$ K. (a) Change in the photocurrent integrated from 3 to 19 μs after a mw excitation for 32 magnetic field values. The mw pulse length was varied from 0 to 510 ns with an increment of 2 ns. The oscillations reflect the coherent spin nutation of the spin-pair ensemble during the mw pulse. The oscillation frequency $\Omega/2\pi$ is 23(2) MHz which corresponds to the Rabi frequency of a spin 1/2 under the conditions used in the experiment. The inset shows the Rabi frequencies determined by Fourier transformation of the coherent oscillations for several mw power levels. The solid line represents a linear fit through the origin. (b) Cut through the data displayed in (a) along the dashed line corrected for a linear baseline. To evaluate the Rabi decay quantitatively, the maxima and minima of the oscillations (marked by the bullets) were fitted with two exponential functions each (solid lines). (c) Difference between maxima and minima in plot (b) versus τ. The solid line shows a fit to the experimental data assuming a single exponential decay (time constant $\tau_{dec}\approx 100$ ns) and a constant offset (≈ 0.05).

oscillations originate from spin Rabi oscillations of charge carriers that are involved in the spin-dependent hopping via localized conduction-band tail and phosphorus states in a-Si:H.[19]

A Fourier transformation of $Q(\tau)$ yields the associated Rabi frequencies. The inset of Fig. 4(a) displays the frequencies determined at four different amplitudes, B_1, of the mw magnetic field. The B_1 axis has been scaled according to Rabi's formula $\Omega=\gamma B_1$, where $\Omega/2\pi$ is the Rabi frequency and $\gamma=g\mu_B/\hbar$ is the gyromagnetic ratio, i.e., the ratio between g value, the Bohr magneton, μ_B, and the Planck's constant, $\hbar$. The solid line represents a linear fit through the origin. From the Rabi frequencies it can be inferred that the oscillations shown in Fig. 4(a) correspond to the Rabi frequency of individual $S=1/2$ particles and therefore originate from spin pairs with weak spin-spin (exchange and dipolar) coupling.[10,14,15] In other words, the mw pulse manipulates only one spin of the precursor pair. The two constituents of the associated spin pair are assigned to neutral phosphorus and conduction-band tail states.

To evaluate the decay of the Rabi oscillations, Fig. 4(b) shows a horizontal cut through the data set along the dashed line in Fig. 4(a). Maxima and minima of the oscillation were fitted with two exponential functions each. Figure 4(c) shows the difference of these fits as a function of the mw pulse length τ which represents the oscillation decay (in the following referred to as Rabi decay). This behavior can be well described by a single exponential function with a decay time constant $\tau_{dec}\approx 100$ ns and an additional constant offset (≈ 0.05). The effects (a)–(d) (as mentioned in the introduction) that determine pEDMR echo decay also influence the Rabi decay observed here. In addition, coherent dephasing caused by a distribution of Rabi frequencies can also contribute to the Rabi decay. Discriminating between these effects is the aim of the rotary echo experiment described in the following section.

V. EXPERIMENTAL OBSERVATION OF ROTARY ECHOES

Using identical experimental conditions as before (see Figs. 3 and 4), a rotary echo experiment as described in Sec. II was performed. For this purpose, $Q(\tau_2)$ was recorded for τ_{off} varying between 0 and 200 μs. The length of pulse 1 was fixed at $\tau_1=136$ ns which corresponds to a flip angle of $\phi=\Omega\cdot\tau_1=5\pi$. The length of pulse 2 was increased from $\tau_2=0$ to 254 ns with an increment of 2 ns. Figure 5(a) shows the signal $Q(\tau_2)$ that was obtained by integrating ΔI_{ph} in the interval from 3 to 19 μs after pulse 2 has ended.

The maximum echo signal occurs, as expected, when both pulses have the same length, i.e., for $\tau_2=\tau_1$. With increasing waiting time we clearly observe in Fig. 5(a) that the maximum due to the echo signal changes into a minimum at $\tau_{off}\approx 10$ μs.

The signal at $\tau_{off}=0$ [uppermost curve in Fig. 5(a)] can approximately be described by an oscillation that is symmetrical to $\tau_2-\tau_1=0$. It represents the echo decay contribution to the EDMR signal, Q_{ed}, that arises from refocused spin pairs. This contribution decreases with increasing τ_{off} due to annihilation of spin pairs between both pulses. Since there is no delay between both pulses here ($\tau_{off}=0$), we can neglect spin-dependent generation. By assuming an exponential damping of the amplitude, the model function can be written as

$$Q_{ed}=A_{ed}-B_{ed}\cos(\omega\cdot|\tau_2-\tau_1|+\phi_{ed})\cdot e^{-|\tau_2-\tau_1|/d_{ed}} \quad (1)$$

with B_{ed} being the amplitude of the oscillation, ω is the Rabi frequency, and ϕ_{ed} is an additional phase factor. d_{ed} denotes the time constant of the exponential damping and A_{ed} is a constant offset. All these parameters are determined by a least square fit. The only parameter that depends on τ_{off} is the amplitude B_{ed}.

Similarly, the signal Q_{np} that originates from new pairs generated during $\tau_{off}=200$ μs [lowermost curve in Fig. 5(a)], can approximately be described by

$$Q_{np}=A_{np}+B_{np}\sin(\omega\cdot\tau_2+\phi_{np})\cdot e^{-\tau_2/d_{np}}. \quad (2)$$

This expression ignores refocused spin pairs (Q_{ed}) and, therefore, B_{np} denotes the amplitude of the damped Rabi oscillation carried out by spin pairs that were generated during τ_{off}. The meaning of the parameters A_{np}, ω, ϕ_{np}, and d_{np} is analogous to the corresponding echo decay parameters defined above.

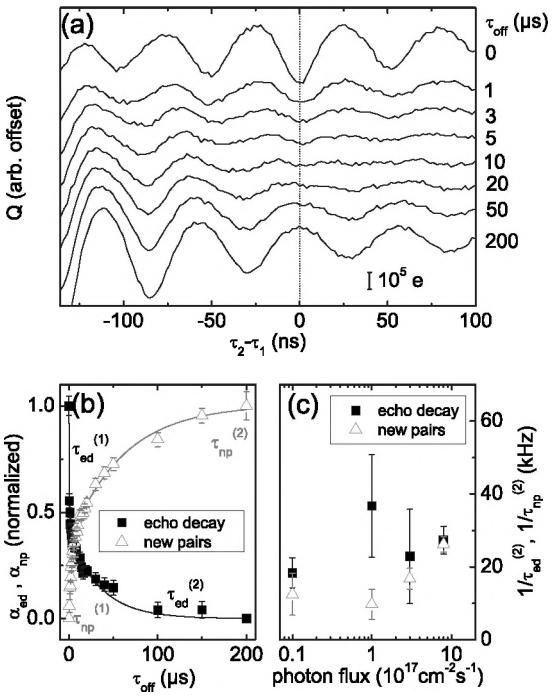

FIG. 5. Results of the pEDMR rotary echo experiment. The experimental conditions are the same like for the previously shown pEDMR results. (a) Charge Q resulting from the integration of the current change between 3 and 19 μs after the second mw pulse as a function of the length of pulse 2. The individual curves correspond to different values of τ_{off} as indicated on the right side of the plot. The sensitivity of the measurement can be estimated from the bar that represents the charge of 10^5 electrons. The condition where the maximum refocusing of the spins occurs ($\tau_1=\tau_2$) is marked by the dotted vertical line. (b) Coefficients α_{ed} and α_{np} representing the contributions to the signal due to echo decay and during τ_{off} generated precursor pairs, respectively. These coefficients were extracted from the data displayed in (a) with a procedure described in the text. The solid lines show best fits using two biexponential functions for the description of the echo decay as well as the signal caused by new spin pairs as a function of τ_{off}. For the four time constants as displayed next to the fit curves we obtain $\tau_{ed}^{(1)}=(0.46\pm0.06)\mu$s, $\tau_{ed}^{(2)}=(35\pm3)\mu$s, $\tau_{np}^{(1)}=(2.9\pm0.3)\mu$s, and $\tau_{np}^{(2)}=(60\pm6)\mu$s. (c) Rate coefficients (inverse of the slow time constants $\tau_{ed}^{(2)}$ and $\tau_{np}^{(2)}$) for several light intensity levels. To obtain these data points, the laser power was varied between 5 and 400 mW corresponding to a photon flux between approximately 10^{16} and 8×10^{17} cm^{-2} s^{-1}.

After determining these parameters by a least square fit, $Q(\tau_2)$ for each value of τ_{off} can be interpreted as a superposition of both contributions Q_{ed} and Q_{np}. Using this phenomenological approach, the EDMR echo signal for each τ_{off} can be described by

$$Q(\tau_2)=\alpha_{ed}\cdot Q_{ed}+\alpha_{np}\cdot Q_{np}+C \tag{3}$$

with Q_{ed} and Q_{np} being the contributions that arise from echo decay and new spin pairs which are given by the expressions in Eqs. (1) and (2). The parameters α_{ed} (echo decay determined by spin-pair annihilation) and α_{np} (signal caused by generation of new pairs) are the respective prefactors that weight the two contributions. C is an additional constant offset.

Thus, by determining the parameters α_{ed} and α_{np} from a fit to the experimentally obtained data for τ_{off} between 0 and 200 μs, a disentanglement of the contributions of spin-pair annihilation and precursor pair generation can be achieved. Figure 5(b) displays these values as a function of τ_{off}. The solid lines represent fits with functions describing a biexponential decay and increase with time constants $\tau_{ed}^{(1)}$, $\tau_{ed}^{(2)}$ and $\tau_{np}^{(1)}$, $\tau_{np}^{(2)}$, respectively. For the light intensity used in this experiment we find $\tau_{ed}^{(1)}=(0.46\pm0.06)$ μs, $\tau_{ed}^{(2)}=(35\pm3)$ μs, $\tau_{np}^{(1)}=(2.9\pm0.3)$ μs, and $\tau_{np}^{(2)}=(60\pm6)$ μs.

Note that the equations for $Q(\tau_2)$ as given above represent only a phenomenological description of the echo signal which is valid for small spin couplings. A more precise expression taking into account the coupling of the spin pairs can be found in Ref. 10. Note further that the good agreement between the biexponential fits and the experimentally found dependence of α_{ed} and α_{np} on τ_{off} does not exclude other models which can correctly describe the experimental data. Reasonably good fits can also be achieved when assuming a distribution of spin-pair annihilation and formation rates which results in a stretched exponential behavior. This is anticipated since stretched exponentials are convolutions of more than two exponentials used for the fit with a biexponential decay.

Figure 5(c) shows the inverse of the slow time constants, namely, the rate coefficients $r_{ed}^{(2)}=1/\tau_{ed}^{(2)}$ and $r_{np}^{(2)}=1/\tau_{np}^{(2)}$, obtained from similar measurements carried out at different light intensities. Changing of the photon flux was accomplished by adjusting the laser power. Thereby, the generation rate of free charge carriers (not necessarily the precursor pair-generation rate) could be varied. Surprisingly, we observe that neither the time constant related to the generation process nor the time constant describing the echo decay change significantly, although the photon flux was varied over almost two orders of magnitude [see Fig. 5(c)]. We have restricted this analysis to the slow time constants (with upper index 2) because the smallest value of τ_{off} used in this study was 500 ns and thus too long to deduce reliable values for the fast time constants $\tau_{ed}^{(1)}$ and $\tau_{np}^{(1)}$ which are indispensable for a thorough analysis. Note that the observation of only weak light intensity dependence and therefore only weak charge-carrier density dependence can be understood by pair formation at defect sites (following Shockley, Read, and Hall) when the charge-carrier generation rate is high enough to saturate almost all defects in the steady state. As the pair-generation rate will approach the pair decay rate under these conditions, the carrier density will only slightly influence the carrier capture and thus the pair formation.

VI. DISCUSSION AND CONCLUSION

The Rabi oscillations shown in Fig. 4 decay exponentially with a time constant of approximately 100 ns. That is significantly smaller than $\tau_{ed}^{(1)}=(0.46\pm0.06)$ μs, i.e., the fastest time constant describing the echo decay. This is in accordance with the finding from a previous study[4] that the damping of the oscillations is mainly caused by Rabi dephasing

due to a distribution of g values or B_1, whereas the effect of annihilation of spin pairs plays only a minor role on the time scale of the mw pulse (the maximum pulse length for the data shown in Fig. 4 was approximately 500 ns). Hence, refocusing of spins with an echo experiment is possible and, thus, the requirement for the application of the presented rotary echo experiment is fulfilled.

The contributions to the echo signal caused by refocused spin pairs (given by α_{ed}) and during τ_{off} generated pairs (given by α_{np}) can clearly be separated by taking advantage of the phase difference between the corresponding pEDMR signals. The dependence of both parameters on τ_{off} can be approximated when assuming two biexponential functions, which might indicate that both spin-pair annihilation and generation are determined by at least two different processes each. In the case of τ_{ed}, two time constants appear if the annihilation rate out of pure triplet states $|\uparrow\uparrow\rangle$ and $|\downarrow\downarrow\rangle$ is different from the rate out of states $|\uparrow\downarrow\rangle$ and $|\downarrow\uparrow\rangle$ with mixed symmetry.[10] These rates are the same that enter the expressions for the pEDMR transients. However, as indicated in Fig. 3(b), the shape of pEDMR transients can be affected by spin-independent influences such as RC constants of the detection electronics or the sample itself, even when there is no change in the dynamics of the spin-dependent processes. While the time constants extracted from pEDMR transients show a strong dependence on the photon flux [see Fig. 3(b)], the time constants deduced from the echo experiment are only slightly affected [cf. Fig. 5(c)], although the laser power was varied over almost two orders of magnitude. Taking into account that the concentration of electrons in the conduction band of the amorphous silicon is approximately proportional to the photon flux,[32] the pEDMR signal shows no pronounced dependence on the concentration of conduction electrons. For a quantitative analysis of the fast echo decay, a more detailed study of the signal at small waiting times ($\tau_{\text{off}} < 500$ ns) is needed, particularly to evaluate the influence of Larmor dephasing and to distinguish between different models (biexponential increase/decay or stretched exponential) that could both explain echo decay and spin-pair generation in accordance with the presented experimental results. It shall be pointed out that the independence of the precursor pair generation and decay times could indicate that both rates are density of state limited processes in contrast to a charge-carrier density-limited processes.

The above interpretation of the experimental results is based on the assumption that the signal Q_{np} is solely determined by spin pairs that were indeed generated during τ_{off}. This assumption is clearly justified when the first pulse is strong enough to excite the whole resonance line. However, due to experimental constraints we were not able to excite the whole line when using a flip angle of $\Omega\tau_1 = 5\pi$ as we did in the experiment. In our case, we used $\tau_1 = 136$ ns for the first pulse. The "natural" linewidth of the EDMR resonance, i.e., the linewidth one obtains without artificial power broadening (at low B_1) is ≈ 1.1 mT. From a comparison of this value with the excitation width that results from τ_1, it is apparent that only $\approx 38\%$ of the resonance line is excited. Consequently, spin pairs from the part of the spectrum which is not in resonance during the first pulse might become resonant during τ_{off} by spectral diffusion[11] and thus also contribute to Q_{np}. Hence, spins that are excited can change the local field (through dipolar interaction) at the position of an initially not excited spin. Since dipolar interaction strongly depends on the distance between the respective spins, we would expect this effect to exhibit a strong dependence on the spin concentration in the tail states which in turn depends on the light intensity. This is not observed in the experiments. Other forms of spectral or instantaneous diffusion could, in principle, influence the echo decay signal (Q_{ed}) but not Q_{np}. Moreover, we want to emphasize that spectral diffusion does only marginally influence spin-lattice relaxation and as the detected rotary echo decay is spin-lattice relaxation dependent,[10] we anticipate that spectral diffusion does not affect the generation rates extracted from the echo experiment.

The connection between experimentally observed EDMR signals and their microscopic origin is not always apparent because different processes such as spin-dependent recombination, hopping transport, and scattering can provoke similar signals[9,16,33] if they involve paramagnetic centers with identical or similar g values. Independent of the microscopic mechanism, the echo experiment opens the possibility to study spin-pair generation provided that the change in conductivity is indeed influenced by spin pairs. This is especially relevant for organic semiconductors, where fundamentally different models for the formation of polaron (spin) pairs exist.[34,35] It has recently been demonstrated that pEDMR can successfully applied to organic light-emitting diodes[5] to measure Rabi oscillations, which is the basis for the rotary echo experiment.

For the quantitative description of pEDMR transients, spin-pair generation is usually taken into account in the form of a constant rate that is equal for all four eigenstates of the spin pair.[4,10] However, there are indications that, at least in some systems, the generation rate could be different for the pure triplet states and the states with mixed symmetry.[36] Thus, the rotary echo experiment could be used to test the validity of this general assumption.

VII. SUMMARY

In summary, we have demonstrated an electrically detected rotary echo experiment which allows the observation of precursor pair formation of spin-dependent electronic transitions through localized states in semiconductors. We have applied the rotary echo experiment to a heterostructure solar cell in order to analyze the influence of spin-pair generation on the pEDMR signal. No significant influence of the spin-pair generation rate on the light intensity was found for the case of a hopping process via conduction-band tail and phosphorus states in a 20-nm-thick layer of amorphous silicon.

ACKNOWLEDGMENTS

We are grateful to Manfred Schmidt, Karsten von Maydell, and Kerstin Jacob for sample preparation. We thank Alexander Schnegg and Matthias Fehr for helpful discussions.

*jan.behrends@helmholtz-berlin.de

[1] W. Shockley and W. T. Read, Jr., Phys. Rev. **87**, 835 (1952).
[2] N. F. Mott, *Metal-Insulator Transitions*, 2nd ed. (Taylor & Francis, London, 1990).
[3] E. L. Frankevich, Chem. Phys. **297**, 315 (2004).
[4] C. Boehme and K. Lips, in *Charge Transport in Disordered Solids with Applications in Electronics*, edited by S. Baranovski (Wiley, Chichester, England; Hoboken, NJ, 2006).
[5] D. R. McCamey, H. A. Seipel, S. Y. Paik, M. J. Walter, N. J. Borys, J. M. Lupton, and C. Boehme, Nature Mater. **7**, 723 (2008).
[6] P. A. Bobbert, T. D. Nguyen, F. W. A. van Oost, B. Koopmans, and M. Wohlgenannt, Phys. Rev. Lett. **99**, 216801 (2007).
[7] M. Reufer, M. J. Walter, P. G. Lagoudakis, B. Hummel, J. S. Kolb, H. G. Roskos, U. Scherf, and J. M. Lupton, Nature Mater. **4**, 340 (2005).
[8] D. Kaplan, I. Solomon, and N. F. Mott, J. Phys. (Paris), Lett. **39**, L51 (1978).
[9] M. Stutzmann, M. S. Brandt, and M. W. Bayerl, J. Non-Cryst. Solids **266-269**, 1 (2000).
[10] C. Boehme and K. Lips, Phys. Rev. B **68**, 245105 (2003).
[11] A. Schweiger and G. Jeschke, *Principles of Pulse Electron Paramagnetic Resonance* (Oxford University Press, Oxford, UK, 2001).
[12] C. Boehme and K. Lips, Phys. Rev. Lett. **91**, 246603 (2003).
[13] A. R. Stegner, C. Boehme, H. Huebl, M. Stutzmann, K. Lips, and M. S. Brandt, Nat. Phys. **2**, 835 (2006).
[14] V. Rajevac, C. Boehme, C. Michel, A. Gliesche, K. Lips, S. D. Baranovskii, and P. Thomas, Phys. Rev. B **74**, 245206 (2006).
[15] A. Gliesche, C. Michel, V. Rajevac, K. Lips, S. D. Baranovskii, F. Gebhard, and C. Boehme, Phys. Rev. B **77**, 245206 (2008).
[16] C. Boehme, J. Behrends, K. V. Maydell, M. Schmidt, and K. Lips, J. Non-Cryst. Solids **352**, 1113 (2006).
[17] K. Lips, C. Boehme, and T. Ehara, J. Optoelectron. Adv. Mater. **7**, 13 (2005).
[18] C. Boehme and K. Lips, J. Mater. Sci.: Mater. Electron. **18**, 285 (2007).
[19] C. Boehme and K. Lips, J. Non-Cryst. Solids **338-340**, 434 (2004).
[20] C. Boehme and K. Lips, Appl. Magn. Reson. **27**, 109 (2004).
[21] H. Huebl, F. Hoehne, B. Grolik, A. R. Stegner, M. Stutzmann, and M. S. Brandt, Phys. Rev. Lett. **100**, 177602 (2008).
[22] K. v. Maydell, E. Conrad, and M. Schmidt, Prog. Photovoltaics **14**, 289 (2006).
[23] J. Schmidt and I. Solomon, C. R. Seances Acad. Sci., Ser. B **263**, 169 (1966).
[24] D. J. Lepine, Phys. Rev. B **6**, 436 (1972).
[25] W. Fuhs, J. Non-Cryst. Solids **354**, 2067 (2008).
[26] J. Behrends, A. Schnegg, C. Boehme, S. Haas, H. Stiebig, F. Finger, B. Rech, and K. Lips, J. Non-Cryst. Solids **354**, 2411 (2008).
[27] R. C. Fletcher, W. A. Yager, G. L. Pearson, A. N. Holden, W. T. Read, and F. R. Merritt, Phys. Rev. **94**, 1392 (1954).
[28] M. Stutzmann and R. A. Street, Phys. Rev. Lett. **54**, 1836 (1985).
[29] M. S. Brandt and M. Stutzmann, Phys. Rev. B **43**, 5184 (1991).
[30] R. Müller, P. Kanschat, S. von Aichberger, K. Lips, and W. Fuhs, J. Non-Cryst. Solids **266-269**, 1124 (2000).
[31] J. Behrends, A. Schnegg, M. Fehr, A. Lambertz, S. Haas, F. Finger, B. Rech, and K. Lips, Philos. Mag. (to be published).
[32] A. Vomvas and H. Fritzsche, J. Non-Cryst. Solids **97-98**, 823 (1987).
[33] C. C. Lo, J. Bokor, T. Schenkel, A. M. Tyryshkin, and S. A. Lyon, Appl. Phys. Lett. **91**, 242106 (2007).
[34] E. L. Frankevich, A. A. Lymarev, I. Sokolik, F. E. Karasz, S. Blumstengel, R. H. Baughman, and H. H. Horhold, Phys. Rev. B **46**, 9320 (1992).
[35] E. J. W. List, C. H. Kim, A. K. Naik, U. Scherf, G. Leising, W. Graupner, and J. Shinar, Phys. Rev. B **64**, 155204 (2001).
[36] F. H. L. Koppens, C. Buizert, K. J. Tielrooij, I. T. Vink, K. C. Nowack, T. Meunier, L. P. Kouwenhoven, and L. M. K. Vandersypen, Nature (London) **442**, 766 (2006).